ELSEVIER

Journal of Molecular Catalysis A: Chemical 166 (2001) 293–302

JOURNAL OF MOLECULAR CATALYSIS A: CHEMICAL

www.elsevier.com/locate/molcata

Electrocatalytic behavior of the $Co_{33}Zr_{67}$ metallic glass for hydrogen evolution☆

A. Jukic, J. Piljac, M. Metikoš-Hukovic*

Department of Electrochemistry, Faculty of Chemical Engineering and Technology, University of Zagreb, P.O. Box 177, 10000 Zagreb, Croatia

Received 18 May 2000; accepted 20 September 2000

Abstract

Amorphous $Co_{33}Zr_{67}$ alloy, prepared by rapid solidification of its components (Co, Zr) in an argon atmosphere, was investigated in view of its possible application as electrocatalytic material for the hydrogen evolution reaction (h.e.r.). Electrocatalytic efficiency was evaluated on the basis of electrochemical and impedance measurements carried out in deaerated 1 M NaOH solution.

The results were compared with polycrystalline Co and Zr metals. The Tafel slope, b_c and the value of exchange current density, j_0 confirmed rather good electrocatalytic properties of Co; on the contrary, pure Zr exhibited very poor activity for the h.e.r. which was influenced by the presence of a ZrO_2 surface layer due to high affinity of Zr for oxygen.

Improved electrocatalytic performances were obtained after the as quenched $Co_{33}Zr_{67}$ samples were chemically pretreated in HF solution. The true kinetic parameters of these electrodes for the hydrogen evolution reaction resembled that of Co, but the stability and activity in the highest state exceeded those of pure polycrystalline Co electrode.

Experimental results of hydrogen evolution kinetics on the $Co_{33}Zr_{67}$ alloy were discussed using known electronic structure of Co–Zr amorphous alloys, ionicity difference between Co and Zr, as well as the free energy of adsorption and the bond strength of hydrogen adsorbed on Co.

Keywords: Co; Zr; Co–Zr alloys; Metallic glasses; Electrocatalysis; Hydrogen evolution; Electronic structure

1. Introduction

The hydrogen evolution reaction (h.e.r.) has thus far been investigated on cobalt electrodes (catalysts) in both alkaline and acidic media [1–3]. Electrocatalytic cobalt materials have been produced under different electrodeposition conditions. A significant decrease in the h.e.r. overpotential was observed for the highly porous and active cobalt electrodes, deposited in the presence of bubbling oxygen and chloride ions, in contrast to cobalt electrodes deposited in a bubbling nitrogen bath. Miao and Piron [4] observed that Ni, Co and Fe composite coatings prepared by electrolytic codeposition were catalytically more active for the h.e.r. than the Ni coated electrode deposited under the same conditions. High electrocatalytic activities of composite-coated electrodes resulted from larger real surface areas of the electrodes, which were dependent on electrodeposition conditions. Bozzini et al. [5] tested various thin films of Co-based Pt, Pd, P and Ni–P alloys, deposited by electrochemical and autocatalytic chemical deposition, as cathodes for the h.e.r. in alkaline solutions. They found that Co–Pt and Co–Pd thin film alloys with low Pt and

☆ Paper presented at the 50th ISE Meeting, Pavia, Italy, 5–10 September 1999.

* Corresponding author. Tel.: +385-1-4597-140; fax: +385-1-4597-139.
E-mail address: mmetik@marie.fkit.hr (M. Metikoš-Hukovic).

1381-1169/01/$ – see front matter
PII: S1381-1169(00)00452-0

high Pd content exhibited the lowest h.e.r. overvoltage among the Co-based films tested. According to Fan et al. [3] the cobalt–nickel–molybdenum catalysts, deposited on a stainless steel screen, enhanced the h.e.r. in alkaline water electrolysis more than the cobalt, nickel, cobalt–molybdenum and nickel–molybdenum deposited catalysts. In comparison to Ni–Mo and Co–Mo, the improvement in electrocatalytic performance on Ni- and Co-based ternary materials was attributed to their large surface area.

Investigations have also extended to catalytic behavior of the cobalt-oxide electrodes for hydrogen evolution. Trasatti and coworkers [6,7] investigated the mechanistic and electrocatalytic aspects of H_2 evolution from alkaline solutions using Co_3O_4 and RuO_2 doped Co_3O_4 electrodes prepared by thermal decomposition of cobalt nitrate. Presented results have shown that Co_3O_4 electrodes were not very active for cathodic H_2 evolution in alkaline solution. Doping Co_3O_4 with RuO_2 increased the electrocatalytic activity of mixed oxides for the h.e.r., with a maximum at intermediate RuO_2 contents.

Due to their mechanical and chemical stability and high electrocatalytic activity, nickel and nickel-based electrodes are among the most often used electrode materials for alkaline water electrolysis [8–11]. Because of its fundamental and technological importance in electrochemistry, hydrogen evolution was extensively studied on a variety of nickel-based hypo-hyper-d-electronic transition metal alloy electrodes [12–20]. The electrocatalytic activity of amorphous $Zr_{100-x}Ni_x$ alloys (metallic glasses), with $x = 33$, 40 and 60, was studied in relation to both, composition and active surface area [21,22]. Kinetic parameters of the hydrogen evolution reaction were evaluated by electrochemical and impedance spectroscopy techniques in 1 M NaOH solution. Electrocatalytic activity of investigated alloys was directly related to the split-band electronic structure of Zr–Ni alloys [23].

In the present work, as quenched and chemically etched $Co_{33}Zr_{67}$ metallic glass electrodes obtained by rapid solidification were studied as catalysts for the hydrogen evolution reaction in 1 M NaOH, at room temperature [24]. The Co–Zr metallic glasses are binary alloys of early (hypo)-late (hyper) transition metals with well-defined electronic structure, physico-chemical and structural properties. Previous studies [25] investigated the influence of hydrogen doping on microhardness, magnetic and electron transport properties of Co–Zr glasses. We reported the results regarding the hydrogen evolution reaction (h.e.r.) on the $Co_{33}Zr_{67}$ amorphous alloy electrode as well as on spectroscopically pure polycrystalline Co and Zr electrodes, in order to characterize alloy electrocatalytic efficiency and stability. The relations between the electrocatalytic performance of the investigated electrodes, their electronic structure and surface conditions, were discussed.

The h.e.r. proceeds via a three-step reaction mechanism in alkaline solutions:

$$M + H_2O + e^- \underset{k_{-V}}{\overset{k_V}{\rightleftharpoons}} MH_{ads} + OH^- \quad (1)$$

$$MH_{ads} + H_2O + e^- \underset{k_{-H}}{\overset{k_H}{\rightleftharpoons}} H_2 + M + OH^- \quad (2)$$

$$MH_{ads} + MH_{ads} \underset{k_{-T}}{\overset{k_T}{\rightleftharpoons}} H_2 + 2M \quad (3)$$

where steps (2) and (3) can take place simultaneously or interchangeably. Steps (1), (2) and (3) are known as the Volmer, Heyrovsky and Tafel reactions. In this reaction mechanism, M represents the electrode material and MH the hydrogen adsorbed on the electrode surface.

2. Experimental

Ribbons of $Co_{33}Zr_{67}$ metallic glass (typically 30 μm thick and 3 mm wide) were prepared by rapid solidification of components (cobalt, zirconium) with more than 99.5% purity level, on a single-roll spinning copper wheel in an argon atmosphere. The structures of the as quenched samples were examined by X-ray diffraction using Cu Kα radiation to confirm that they were amorphous. For comparison, electrochemical tests were performed on polycrystalline, spectroscopically pure Co and Zr electrodes. The exposed faces of investigated electrodes were polished to a mirror finish with Buehler 0.05 μm alumina powder, and rinsed with distilled water and alcohol.

Surface activation treatments have been performed on the amorphous $Co_{33}Zr_{67}$ alloy electrode by chemical etching, for 60 s with 1 M aqueous HF, at room temperature.

All experiments were carried out at room temperature (298 K) in deaerated 1 M NaOH aqueous solution, using quasi-potentiostatic polarization and ac impedance spectroscopy techniques. The solution was deaerated by continuous bubbling with purified nitrogen. The dc polarization curves and ac impedance spectra were measured using the corrosion measurement software (CorrWare®) and the electrochemical impedance software (ZPlot®) with a Solartron model 1287 Electrochemical Interface and a Solartron model 1255 Frequency Response Analyzer.

Polarization curves and impedance spectra were recorded after keeping the electrodes at a constant current density of $-1\,\mathrm{mA\,cm^{-2}}$ for 1800 s. The electrode potential attained at this current corresponds to the hydrogen evolution reaction. The impedance spectra were recorded in a frequency range from 100 kHz to 0.1 Hz using 5 mV peak-to-peak amplitude. The selected applied dc potentials were located mainly in the linear portion of the Tafel lines. The solution resistances between the tested electrode and the reference electrode were determined by ac impedance measurement. Ohmic drop corrections, based on these resistances, were applied in all polarization measurements.

A standard three-electrode cell was utilized in all measurements, the counter electrode was a large-area platinum electrode and the reference electrode was a saturated calomel electrode (SCE).

3. Results and discussion

3.1. Polarization measurements

Amorphous $Zr_{67}Co_{33}$ alloy electrode, in the as quenched state and pretreated in aqueous hydrofluoric acid, as well as polycrystalline, spectroscopically pure Co and Zr electrodes, were investigated for the hydrogen evolution reaction. Quasi-potentiostatic curves were recorded in the potential range between the H_2 reversible potential, −1.068, and −1.5 V versus SCE, at the scan rate of $1\,\mathrm{mV\,s^{-1}}$.

As a measure of catalytic efficiency, the Tafel slopes and exchange current densities were derived from such plots. Data fitting was performed by the least-squares regression analysis of experimental j against E data

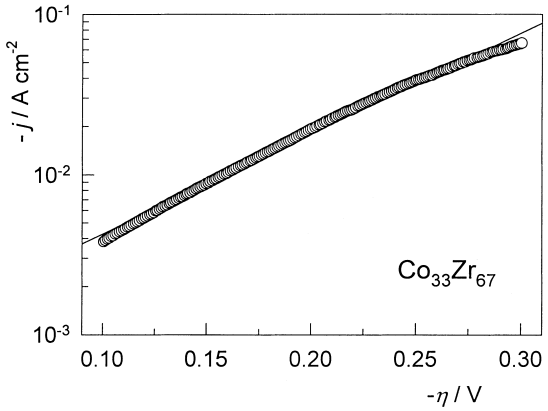

Fig. 1. Quasi-potentiostatic cathodic polarization curve for as quenched $Co_{33}Zr_{67}$ amorphous alloy in 1 M NaOH at room temperature. The full line represents the calculated curve while points stand for experimental results.

based on the relevant equation, in exponential form [26]:

$$j = j_0 \exp \frac{\alpha \eta F}{RT} = j_0 \exp \frac{\eta}{b_c} \tag{4}$$

where j is the current density, j_0 the corresponding exchange current density, α the charge transfer coefficient (used value was 0.5), η the overpotential, and b is the Tafel slope. Fig. 1 shows as an example a comparison between the calculated and experimental Tafel plots for the as quenched $Co_{33}Zr_{67}$ electrode, after correction for an uncompensated IR drop. Points stand for experimental results, while the full line represents the calculated curve for a Volmer–Heyrovsky mechanism, Eq. (2), as the rate determining step, r.d.s. The current density was calculated using the geometric area of the electrodes. Table 1 contains the obtained kinetic parameters for the hydrogen evolution reaction.

For the cobalt electrode, at overpotentials higher than −0.2 V, the Tafel slope of $0.123\,\mathrm{V\,dec^{-1}}$ is close to the theoretical value of $0.118\,\mathrm{V\,dec^{-1}}$ for the h.e.r. at 298 K, according to the Volmer–Heyrovsky mechanism. A relatively high Tafel slope of $0.237\,\mathrm{V\,dec^{-1}}$ for the as quenched $Co_{33}Zr_{67}$ electrode and a very high Tafel slope of $b_c = 0.667\,\mathrm{V\,dec^{-1}}$ for the Zr electrode clearly indicate the presence of a surface oxide film on these electrodes. Surface analysis by the XPS technique has shown that Zr exists as an electrocat-

Table 1
Kinetic parameters for the h.e.r. for the Co and chemically pre treated (∗) $Co_{33}Zr_{67}$ electrodes in 1 M NaOH, at room temperature, deduced from (A) measured polarization curves, based on the geometric surface area and (B) electrochemical impedance spectroscopy measurements, based on the real surface area

	A		B	
	Co	$Co_{33}Zr_{67}$∗	Co	$Co_{33}Zr_{67}$∗
b_c ($V\,dec^{-1}$)	0.123	0.149	0.097	0.120
j_0 ($A\,cm^{-2}$)	8.40×10^{-6}	8.55×10^{-4}	3.976×10^{-8}	1.872×10^{-7}

alytically inert oxide of ZrO_2 on the electrode surface [22].

The Tafel slopes, greater than $2.3 \times 2RT/F = 118$ mV (at room temperature), are usually regarded as anomalous since they cannot be predicted for the mechanism, given by Eqs. (1)–(3). Experimentally, it is frequently observed [27] that the values of Tafel slopes obtained are greater than 118 mV for hydrogen evolution reactions proceeding on oxide-covered electrodes. The most successful interpretation, Meyer [28], has been widely accepted and seems to provide a quantitative analysis of the problem. A part of the applied metal-solution overpotential may be assumed to operate across the oxide layer and hence is not available to assist the charge transfer at the film-solution interface. Accordingly, an activation barrier exists for the transport of electrons through the oxide film, and this barrier must be surmounted by application of an electric field in order for the reaction to proceed. In general, it may be assumed that η_f, the potential drop across the oxide film of given thickness and properties, is a function of the total overpotential [29]:

$$\frac{\partial\eta}{\partial \log j} = \frac{2.3RT}{\beta zF(1 - \partial\eta_f/\partial\eta)} \equiv \text{Tafel slope} \qquad (5)$$

where j is the current density, T the absolute temperature, z the valence of the discharging ion, F the Faraday constant, β the charge transfer symmetry factor, η the total metal-oxide-solution overpotential, η_f the fraction of η which operates across the semiconducting oxide film and R the gas constant. In the absence of an oxide film and with the usual values of $\beta = 0.5$ and $z = 1$, the Tafel slope would be 118 mV at room temperature, as expected from theory. The calculated values using anomalous Tafel slopes of 0.667 and 0.237 V dec^{-1} for Zr and $Co_{33}Zr_{67}$ electrodes further yield $\eta_f = 0.82\eta$ and $\eta_f = 0.5\eta$ for the Zr and $Co_{33}Zr_{67}$ electrodes, respectively. It may be concluded from the obtained values that the presence of an oxide on the electrode surface leads to an inhibition of the hydrogen evolution reaction.

Chemical pretreatment in 1 M HF acid for a short time (60 s) significantly enhanced the electrocatalytic activity of the $Co_{33}Zr_{67}$ alloy with an increase in the exchange current density calculated per unit of geometric area and a Tafel slope decrease in comparison to the untreated electrode (Table 1). This was attributed to dissolution of Zr and removal of a thin ZrO_2 oxide film and an enrichment of the electrode surface with cobalt and will be discussed later.

3.2. Impedance spectroscopy measurements

The impedance data were collected at selected applied dc potentials located mainly in the linear portion of the Tafel plots, at an overpotential in the range from −0.05 to −0.45 V.

Figs. 2–4 show impedance diagrams at different overpotentials for the Co electrode and $Co_{33}Zr_{67}$ amorphous alloy electrode, before and after chemical pretreatment with 1 M HF. Impedance diagrams are shown in the form of Bode plots (the logarithm of overall impedance modulus, $\log|Z|$ and the phase angle, θ versus the logarithm of frequency, $\log f$).

At intermediate frequencies a linear dependence of $\log|Z|$ against $\log f$ and one well-defined maximum observed in the θ against $\log f$ plot, indicate capacitive behavior of the electrode. At low and high frequencies, a transition from capacitive to resistive behavior is apparent. The θ drops towards zero at both high and low frequencies. The ohmic resistance is the dominating impedance component at the highest frequencies and the value of the electrolyte resistance, R_{el}, can be deduced from the high frequency impedance plateau.

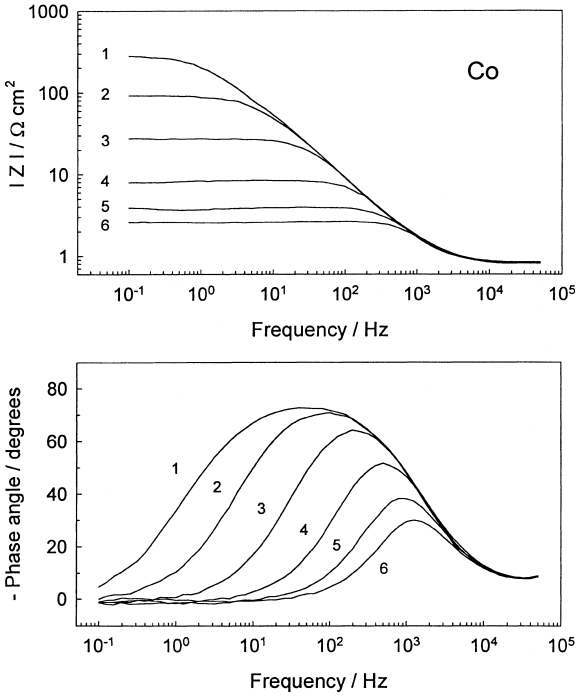

Fig. 2. Impedance spectra (Bode plots) of polycrystalline cobalt electrode for the h.e.r. in 1 M NaOH, at various overpotentials, $-\eta/V$: 0.2 (1), 0.25 (2), 0.3 (3), 0.35 (4), 0.4 (5), 0.45 (6).

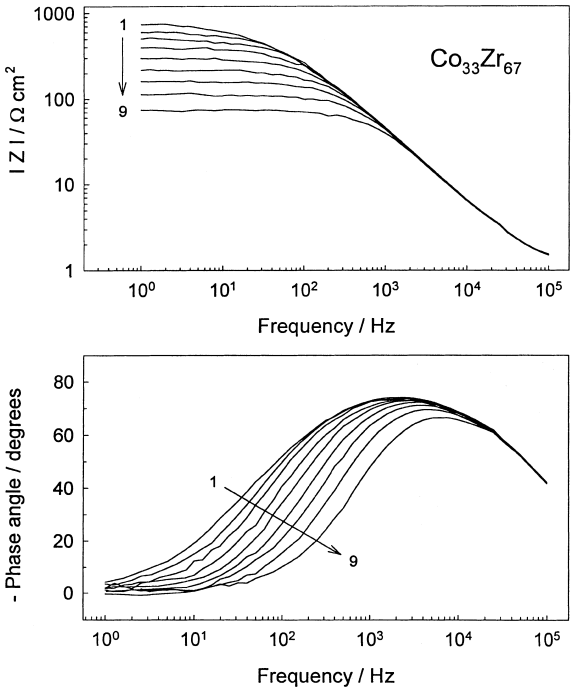

Fig. 3. Impedance spectra (Bode plots) of as quenched $Co_{33}Zr_{67}$ amorphous alloy for the h.e.r. in 1 M NaOH, at various overpotentials, $-\eta/V$: 0.05 (1), 0.1 (2), 0.15 (3), 0.2 (4), 0.25 (5), 0.3 (6), 0.35 (7), 0.4 (8), 0.45 (9).

At the lowest frequencies, the Faradaic resistance i.e. the charge transfer resistance, R_{ct} dominates, which can be obtained from the low frequency impedance plateau as $(R_{el} + R_{ct})$.

It should be noted that charge transfer resistance continuously decreases with increasing overpotential, attaining relatively low values of $R_{ct} \leq 10\,\Omega\,cm^2$, as can be seen in Figs. 2–4. The cobalt electrode exhibits the sharpest drop of R_{ct} with increasing overpotential, indicating a sharp reaction rate increase for the hydrogen evolution process with increasing cathodic potential, see Fig. 2. The low frequency ohmic impedance plateau is the widest at high overpotentials, for Co and $Co_{33}Zr_{67}$ electrodes it extends through more than four decades of the frequency logarithm. At the same time, the frequency region in which capacitive behavior determines the impedance response of the electrode shrinks, indicating a faster hydrogen adsorption–desorption process at the electrode surface during the h.e.r. The resulting values of charge transfer resistance are very low, a few orders of magnitude lower than the ones attained for the untreated electrode. Once selective dissolution and removal of the Zr-oxide component occurs, a cobalt-rich layer remains at the alloy surface, and it acts as an electrocatalyst for rapid activation [19,30].

All the impedance spectra for the treated and untreated $Co_{33}Zr_{67}$ electrode and spectra for the Co electrode at $\eta \geq -0.2$ V, can be well described using only one time constant, characteristic for a purely kinetically controlled reaction. A simple electrical equivalent circuit (EEC) used for the analysis of experimental data, consists of the solution resistance, R_{el}, in series with a parallel connection of the electrode capacitance, C, while the charge transfer resistance, R_{ct}, relates to the hydrogen evolution reaction (Fig. 5). Complex non-linear least squares (CNLLS) programs supplied by Macdonald et al. [31] and Boukamp [32] were used to analyze the real and imaginary impedance components, Z' and Z'', for all frequencies at each dc potential. The values of circuit elements obtained using a CNLLS program are shown in Table 2. The fitting pro-

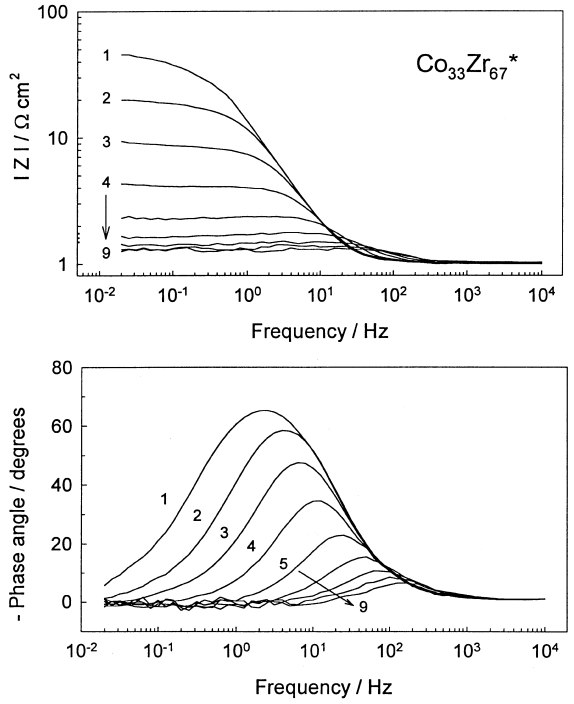

Fig. 4. Impedance spectra (Bode plots) of chemically pre-treated (∗) $Co_{33}Zr_{67}$ amorphous alloy for the h.e.r. in 1 M NaOH, at various overpotentials, $-\eta/V$: 0.05 (1), 0.1 (2), 0.15 (3), 0.2 (4), 0.25 (5), 0.3 (6), 0.35 (7), 0.4 (8), 0.45 (9).

cedure resulted in a very good agreement between experimental and theoretical data. A standard deviation χ-quadrate was of the order of 10^{-4}, and the relative error was less than 5%. The charge transfer resistance is defined as

$$R_{\mathrm{ct}} = \lim_{\omega \to 0} \mathrm{Re}\{Z_{\mathrm{f}}\} \tag{6}$$

where $\mathrm{Re}\{Z_{\mathrm{f}}\}$ denotes the real part of the complex faradaic impedance, Z_{f} and ω is the frequency of the ac signal ($\omega = 2\pi f$). In this model, the total impedance Z is given by

$$Z = R_{\mathrm{el}} + \frac{1}{(R_{\mathrm{ct}}{}^{-1} + \mathrm{j}\omega C_{\mathrm{dl}})} \tag{7}$$

where j is the imaginary number ($\mathrm{j} = \sqrt{-1}$).

With known values of charge transfer resistance, it is possible to calculate the exchange current density, j_0, according to the relation:

$$\left(\frac{\partial \eta}{\partial j}\right)_{\eta \to 0} = \frac{RT}{zF}\frac{1}{j_0} = R_{\mathrm{ct}} \tag{8}$$

The exchange current density is a widely used measure of electrocatalytic activity of any electrode for a particular process. It is important to note here, that for optimum performance of hydrogen cathodes in a water electrolyzer, not only the highest possible values of the exchange current densities, but also low values of Tafel slopes as well as long term stability of the electrode are required.

In order to compare the catalytic activity of different electrodes their surface area must first be assessed and the surface effect subtracted from the apparent activity. The surface roughness factor of the electrodes, proportional to their electrochemically active surface area, was evaluated based on the apparent double-layer capacitances determined by ac impedance measurements. The R_{ct} and C_{exp} parameters included in Table 2 were determined in terms of the geometric area and C_{exp} could be expressed as the sum of pseudocapacitance, C_{ϕ} and double-layer capacitance, C_{dl} [33,34]. Thus,

$$C_{\mathrm{exp}} = C_{\mathrm{dl}} + C_{\phi} \tag{9}$$

In the investigated overpotential range, C_{exp} decreased with increasing overpotential, and tended to remain constant at high h.e.r. overpotentials. At high overpotentials, pseudocapacitance approached zero, and determined C corresponded to the apparent double-layer capacitance, C_{dl}, independent of potential. The surface roughness factor σ for each electrode was calculated by dividing C_{dl} by the double-layer capacitance ($20\,\mu\mathrm{F\,cm^{-2}}$) of a smooth metal surface [35,36].

The surface roughness factor determined by ac impedance measurements was about 6 for the Co electrode. For the smooth $Co_{33}Zr_{67}$ electrode, σ attained a value much smaller than 1 and it was approximately

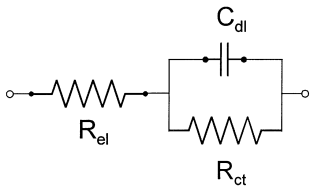

Fig. 5. Electrical equivalent circuit used for simulating the ac impedance spectra for the hydrogen evolution reaction on solid electrodes.

Table 2
Fitted parameter values of the electrical equivalent circuits for Co and as quenched and chemically pre-treated (∗) $Co_{33}Zr_{67}$ electrodes for the h.e.r., in 1 M NaOH solution, at room temperature

	Overpotential, $-\eta/V$						
	0.05	0.1	0.15	0.2	0.25	0.3	0.35
Cobalt							
C_{exp} ($\mu F\,cm^{-2}$)	601	390	328	415	288	182	135
R_{ct} ($\Omega\,cm^2$)	2883	1160	489.5	283.4	91.67	27.37	7.70
As quenched $Co_{33}Zr_{67}$							
C_{exp} ($\mu F\,cm^{-2}$)	6.5	5.4	4.8	4.1	4.1	3.7	3.6
R_{ct} ($\Omega\,cm^2$)	765.6	601.2	479.8	393.5	293.7	206.8	157.8
Chemically pretreated $Co_{33}Zr_{67}$∗							
C_{exp} ($\mu F\,cm^{-2}$)	13756	10469	9731	9248	7731	6102	3395
R_{ct} ($\Omega\,cm^2$)	42.0	17.8	7.59	3.10	1.36	0.74	0.49

180 for the rough, chemically activated $Co_{33}Zr_{67}$ amorphous alloy electrode. An extremely low value of σ for the smooth, as quenched $Co_{33}Zr_{67}$ electrode indicated the existence of an interfacial oxide on the smooth surface of metallic glass and great homogeneity of its amorphous structure. The reduction of the electrode active surface area, with increasing overpotential during the h.e.r., is clearly visible from a decrease in the roughness factor. A decrease in the roughness factor of the as quenched $Co_{33}Zr_{67}$ electrode may be explained by a decrease in the electrode specific capacity probably due to bulk and surface transformation and the formation of hydrogen doped alloy $(Co_{33}Zr_{67})_{1-x}H_x$ [18,25,37].

The dependence of the logarithm of the inverse charge transfer resistance, ${R_{ct}}^{-1}$ on the overpotential, recalculated for the real surface area, is presented in Fig. 6. From this figure, it may be pointed out that in the overpotential range from -0.05 to -0.35 V, the relationship between $\log {R_{ct}}^{-1}$ and η is linear, with a slope $d\eta/d(\log {R_{ct}}^{-1})$ of 97 mV dec^{-1} for the Co electrode and 120 mV dec^{-1} for the chemically treated $Co_{33}Zr_{67}$ electrode. Extrapolating the values of charge transfer resistance to the zero overpotential for the hydrogen evolution reaction ($E_{rev} = -1.068$ V versus SCE), according to the Eq. (8), yields the exchange current densities for the h.e.r. Thus, the values of the exchange current densities, based on the real surface areas, are 3.98×10^{-8} A cm^{-2} for the Co electrode and 1.87×10^{-7} A cm^{-2} for the chemically treated $Co_{33}Zr_{67}$ amorphous alloy electrode. These exchange current density values of the discharge step (2), accompanied with Tafel slope values contained in Table 1, indicate a true electrocatalytic nature of the electrode for the hydrogen evolution reaction.

The exchange current density for chemically treated $Co_{33}Zr_{67}$ electrode is very close to the one for pure cobalt. A comparison of intrinsic activities (true exchange current densities — per unit of real surface area) implies that an increase in the activity of chemically treated $Co_{33}Zr_{67}$ electrode arises from an increase in the surface roughness accompanied by the Co-enriched surface layer. Some amorphous alloys may not be electrocatalytically active in their

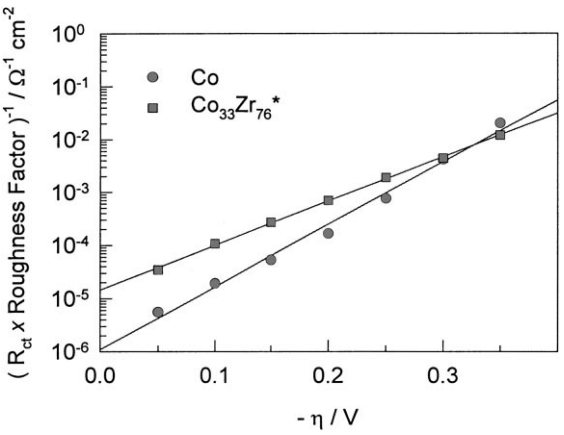

Fig. 6. The logarithm of charge transfer admittance, ${R_{ct}}^{-1}$ for polycrystalline cobalt and chemically pre-treated (∗) $Co_{33}Zr_{67}$ amorphous alloy, as a function of the overpotential, based on the real electrode surface.

as quenched state but their activity can be significantly improved by chemical etching. Thin oxide films, generally produced at the surfaces during rapid quenching, must be removed by chemical etching. Moreover, surface area of as quenched ribbons is very low and can be increased by suitable activation treatments. In the case of Ni-based amorphous alloys, it was shown that a pretreatment with HF significantly enhances the electrocatalytic activity either by removing the surface oxide layers or by increasing the roughness factor [12,30]. Amorphous Cu–Ti, Cu–Zr alloys [38], Ni–Ti, Ni–Zr and Pd–Zr [12,19,21,22,30,39] alloys were found to be electrocatalytically very active for the h.e.r. after treatment in 1 M HF solution. Chemically activated alloys exhibited a much higher reaction rate than their original melt-spun and crystalline counter-parts [30,40]. This improvement was attributed to selective dissolution of TiO_2 and ZrO_2 oxide layers respectively, which left a porous electrocatalytically active Cu, Ni or Pd layer. More information was obtained using in depth analysis of untreated and activated amorphous Ni–Zr alloys (NiZr, $Ni_{36}Zr_{64}$ and $NiZr_2$) [19]. The variation in the Ni^+/Zr^+ and $Zr^+/ZrO_2{}^+$ ratios as a function of sputtering time was reported. It was found that chemical etching with HF clearly enhanced the Ni^+/Zr^+ ratio not only in the surface layers but also in the inner layers of the alloys. SIMS profiles of the $NiZr_2$ alloy [19] confirmed the hypothesis that HF treatment causes preferential dissolution of Zr in the amorphous alloy, resulting in nickel enrichment at the surface. According to the SEM and XRD analyses the treatment (etching) with HF induced formation of crystalline fcc Ni: the preferred orientation of Ni crystals grown at the surface was related to the easy growth direction of fcc metals. The typical shape of (1 1 1) oriented crystals was observed [30].

Enhanced electrocatalytic activity observed for amorphous alloys after chemical treatments was not observed on their crystalline counterparts after similar chemical treatments [40].

Ezaki et al. [41,42] have proposed an electronic model for understanding the alloying effect of transition metal based alloys on the catalytic properties for the h.e.r. Based on the proposed model, catalytic activity for the h.e.r. of Zr binary alloys containing 3d and 4d transition metal elements (M) was evaluated from a series of experiments and electronic structure calculations [20]. The variation in catalytic activity, i.e. hydrogen overpotential, was explained in terms of the charge transfer direction between atoms in the alloy. The negative value of the ionicity difference, $I_M - I_{Zr} = \Delta I$ between M and Zr atoms means that the electron transfer occurs from the surrounding Zr atoms to the atoms of the alloying element M, whereas a positive value of ΔI means that electron transfer occurs in a reversed direction. All 3d and 4d alloying elements had negative ionicity due to electron transfer from base Zr metal to the alloying element. Accordingly, as a result of charge transfer between the constituent atoms, the "negatively" charged atom in the compound was mainly responsible for the hydrogen overpotential change with alloying.

3.3. Electrocatalytic activity of the $Co_{33}Zr_{67}$ amorphous alloy for the h.e.r., based on the electronic structure influence

Based on polarization and impedance results, it was found that catalytic behavior of the alloy resembled that of cobalt much more than that of zirconium. These experimental results were supported by considering the valence-band spectrum of amorphous Co–Zr alloy, the electronic structure calculations of ionicity difference between Co and Zr, $I_{Co} - I_{Zr}$, as well as the work function and the bond strength of hydrogen adsorbed on the surface of Co electrode.

Fig. 7 from reference [43] shows a valence-band spectrum of the $Co_{30}Zr_{70}$ metallic glass obtained by

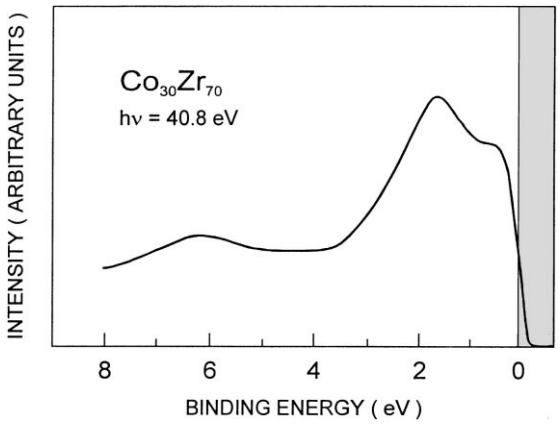

Fig. 7. Valence-band spectrum ($h\nu = 40.8$ eV) of $Co_{30}Zr_{70}$ metallic glass.

ultraviolet photoelectron spectroscopy (UPS) and deconvoluted by electron structure calculations [44]. The structure near the Fermi energy level, E_F, originates mainly from the 4d Zr electrons while the peak at higher binding energies (≈1.4 eV below the Fermi level) is mainly related to the 3d Co electrons. The broad structure located at about 6 eV below the Fermi level [43] is associated with the formation of a surface oxide, ZrO_2 or Zr-hydride. A small displacement of the 3d Co subband position from the Fermi level, $\Delta = -1.4$ eV for the $Co_{30}Zr_{70}$ alloy, indicates that the 3d Co subband has a large contribution at E_F and that the 3d Co states play an important role in determining the catalytic properties of the alloy. The surface layers of amorphous alloy samples (both solid and liquid) are enriched with clusters, characterized by stronger hybridized bonds between the d-electrons of the host lattice of Zr atoms and the d-electrons of the Co doping atoms, which are the cluster-forming elements [45]. Co atoms are more electronegative ($\Delta I = I_{Co} - I_{Zr} = -3.3$) than Zr atoms ($\Delta I = I_{Zr} - I_{Zr} = 0$) and tend to have weaker interaction with hydrogen compared to the positively charged Zr atoms. Since the electrochemical desorption is the rate determining step of the h.e.r., the maximum rate of hydrogen evolution will occur at intermediate values of M–H bond strength. This is indeed observed, in the well known "volcano plot" of exchange current density against M–H bond strength (ΔG^0_{ads}), for a series of metal cathodes [46,47]. Co forms M–H bonds with energies of about 210 kJ mol^{-1} and has a work function of about 4.7 eV. Judging upon the values of the metal work function given by Trasatti [46] and the M–H bond strengths derived by Krishtalik [47], an ideal electrocatalyst lacks two electrons to fill its outermost d and s sublevels, has a work function of about 5 eV, and forms M–H bonds with energies of about 210–250 kJ mol^{-1}.

4. Conclusion

- Electrocatalytic efficiency for the hydrogen evolution reaction on amorphous $Co_{33}Zr_{67}$ alloy was evaluated on the basis of electrochemical and impedance spectroscopy data carried out in deaerated 1 M NaOH solution. For comparison, electrochemical and impedance tests were also performed on polycrystalline Co and Zr metal electrodes.
- The exchange current density, j_0 and Tafel slope, b_c were taken as reasonable measures of catalytic efficiency of investigated materials for the h.e.r.
- The exchange current densities per true unit surface area were obtained from non-linear least square fit of the impedance data (Eqs. (6) and (7)) and were compared with results from an analysis of quasi-potentiostatic polarization curves (Eq. (4)).
- The surface roughness was determined using non-destructive method of capacity measurements.
- The impedance data are consistent with the results obtained from the analysis of polarization curves (electrochemical measurements). Analysis and discussion of the kinetic parameters for the h.e.r. were based on the Volmer–Heyrovsky reaction mechanism.
- Electrocatalytic activity for the h.e.r. of the as-quenched $Co_{33}Zr_{67}$ electrode was lower than that of the Co electrode. Anomalous Tafel slope, $b_c = 230$ mV dec^{-1} can be related to the presence of a thin oxide layer produced at the surface during rapid quenching. A part of the applied potential operates across this oxide layer and hence is not available for the charge transfer reaction at the film/solution interface.
- The increase in electrocatalytic efficiency of the Co–Zr alloy for the h.e.r. after chemical pretreatment in HF solution may be mainly attributed to the increase of surface Co concentration after removal of the Zr surface oxide (as was evidenced by cyclic voltammetry). The stability and electrocatalytic activity of these electrodes, per true unit area in the highest state, exceeded that of pure Co electrode.
- Experimental results of hydrogen evolution kinetics on the $Co_{33}Zr_{67}$ alloy were discussed on the basis of a valence band spectrum of this alloy and electronic structure calculated for Zr-transition metal binary alloys. These alloys have electronic structures which exhibit higher catalytic activity with respect to the parent elements, although lower with respect to noble metals (Pt).

References

[1] M. Rojas, C.L. Fan, H.J. Miao, D.L. Piron, J. Appl. Electrochem. 22 (1992) 1135.
[2] C. Fan, D.L. Piron, H.J. Miao, M. Rojas, J. Appl. Electrochem. 23 (1993) 985.

[3] C. Fan, D.L. Piron, P. Paradis, Electrochim. Acta 39 (1994) 2715.
[4] H.J. Miao, D.L. Piron, Electrochim. Acta 38 (1993) 1079.
[5] B. Bozzini, G. Zangari, P.L. Cavallotti, Electrochim. Acta 39 (1994) 1787.
[6] E. Veggetti, I.M. Kodintsev, S. Trasatti, J. Electroanal. Chem. 339 (1992) 255.
[7] N. Krstajic, S. Trasatti, J. Appl. Electrochem. 28 (1998) 1291.
[8] A. Lasia, A. Rami, J. Electroanal. Chem. 294 (1990) 123.
[9] M.R. Gennero, J. Electroanal. Chem. 448 (1998) 87.
[10] A.N. Correia, S.A.S. Machado, Electrochim. Acta 43 (1998) 367.
[11] J.G. Highfield, E. Claude, K. Oguro, Electrochim. Acta 44 (1999) 2805.
[12] K. Machida, M. Enyo, I. Toyoshima, K. Miyahara, K. Kai, K. Suzuki, Bull. Chem. Soc. Jpn. 56 (1983) 3393.
[13] K. Machida, M. Enyo, G. Adachi, Y. Shiokawa, Electrochim. Acta 29 (1984) 87.
[14] G. Jorge, R. Faure, R. Durand, A.R. Yavari, Mater. Sci. Eng. 99 (1988) 517.
[15] J.Y. Huot, A. van Neste, L. Brossard, R. Schulz, Surf. Coat. Technol. 35 (1988) 241.
[16] J.Y. Huot, M. Trudeau, L. Brossard, R. Schulz, J. Electrochem. Soc. 136 (1989) 2224.
[17] R. Schulz, A. van Neste, L. Brossard, J.Y. Huot, Mater. Sci. Eng. 99 (1988) 469.
[18] R. Simpraga, L. Bai, B.E. Conway, J. Appl. Electrochem. 25 (1995) 628.
[19] E. Angelini, C. Antonione, M. Baricco, S. Daolio, M. Fabrizio, F. Rosalbino, in: Proceedings of the 7th European Conference on Applications of Surface and Interface, Göteborg, 1997, p. 224.
[20] H. Shibutani, T. Higashijima, H. Ezaki, M. Morinaga, K. Kikuchi, Electrochim. Acta 43 (1998) 3235.
[21] A. Jukic, M. Metikoš-Hukovic, in: Proceedings of the 3rd International Symposium on Electrocatalysis: Advances and Industrial Applications, Portorose, Slovenia, 11–15 September, 1999, p. 201.
[22] M. Metikoš-Hukovic, A. Jukic, Electrochim. Acta. Electrochim. Acta 45 (2000) 4159.
[23] A. Amamou, R. Kuentzler, Y. Dossmann, P. Forey, J.L. Glimois, J.L. Feron, J. Phys. F: Met. Phys. 12 (1982) 2509.
[24] A. Jukic, J. Piljac, M. Metikoš-Hukovic, in: Proceedings of the 50th International Society of Electrochemistry Meeting, Pavia, Italy, 5–10 September, 1999, Vol. 1, p. 831.
[25] I. Kokanovic, B. Leontic, J. Lukatela, J. Non-Cryst. Solids 205–207 (1996) 673.
[26] J.O.'M. Bockris, S.U.M. Khan, Surface Electrochemistry: A Molecular Level Approach, Plenum Press, New York, 1993, Chapter 3, p. 211.
[27] M. Metikoš-Hukovic, R. Babic, Z. Grubac, S. Brinic, J. Appl. Electrochem. 24 (1994) 772.
[28] R.E. Meyer, J. Electrochem. Soc. 107 (1960) 847.
[29] A.K. Vijh, J. Electrochem. Soc. 116 (1969) 1323.
[30] S. Spriano, M. Baricco, C. Antonione, E. Angelini, F. Rosalbino, P. Spinelli, Electrochim. Acta 39 (1994) 1781.
[31] J.R. Macdonald, J. Schoonman, A.P. Lehner, J. Electroanal. Chem. 131 (1982) 77.
[32] B.A. Boukamp, Solid State Ionics 20 (1980) 31.
[33] B.V. Tilak, B.E. Conway, Electrochim. Acta 21 (1976) 745.
[34] T. Liu, B.E. Conway, J. Appl. Electrochem. 17 (1987) 983.
[35] L. Chen, A. Lasia, J. Electrochem. Soc. 139 (1992) 3214.
[36] R. Karimi Shervedani, A. Lasia, J. Appl. Electrochem. 29 (1999) 979.
[37] L. Bai, D.A. Harrington, B.E. Conway, Electrochim. Acta 32 (1987) 1713.
[38] K. Machida, M. Enyo, K. Kai, K. Suzuki, J. Less-Common Met. 100 (1984) 377.
[39] M. Enyo, T. Yamazaki, K. Kai, K. Suzuki, Electrochim. Acta 28 (1983) 1573.
[40] K. Lian, D.W. Kirk, S.J. Thorpe, Electrochim. Acta 36 (1991) 537.
[41] H. Ezaki, M. Morinaga, S. Watanabe, Electrochim. Acta 38 (1993) 557.
[42] H. Ezaki, M. Morinaga, S. Watanabe, J. Saito, Electrochim. Acta 39 (1994) 1769.
[43] M. Tenhover, D. Lukco, W.L. Johnson, J. Non-Cryst. Solids 61/62 (1984) 1049.
[44] V.L. Moruzzi, P. Oelhafen, A.R. Williams, R. Lapka, H.-J. Guntherodt, J. Kubler, Phys. Rev. B 27 (1983) 2049.
[45] I.N. Shabanova, A.V. Kholzakov, V.N. Chebotnikov, J.E. Mukhina, in: Proceedings of the 7th European Conference on Applications of Surface and Interface Analysis, Göteborg, 1997, p. 647.
[46] S. Trasatti, J. Electroanal. Chem. 39 (1972) 163.
[47] L.I. Krishtalik, in: P. Dalahay, C. Tobias (Eds.), Advances in Electrochemistry and Electrochemistry Engineering, Vol. 7, Interscience, New York, 1970, p. 283.